Received August 30, 2020, accepted September 14, 2020, date of publication September 18, 2020, date of current version October 2, 2020.

Digital Object Identifier 10.1109/ACCESS.2020.3024697

Bearing Fault Diagnosis Based on Iterative 1.5-Dimensional Spectral Kurtosis

XIONG ZHANG, (Member, IEEE), SHUTING WAN, YULING HE, (Member, IEEE), XIAOLONG WANG, AND LONGJIANG DOU, (Member, IEEE)

Hebei Key Laboratory of Electric Machinery Health Maintenance and Failure Prevention, North China Electric Power University, Baoding 071003, China

Corresponding author: Shuting Wan (zxncepu@163.com)

This work was supported in part by the National Natural Science Foundation of China under Grant 51777075, in part by the Fundamental Research Funds for the Central Universities under Grant 2020MS111 and Grant 2018QN093, and in part by the Natural Science Foundation of Hebei Province under Grant E2019502047.

ABSTRACT The key step of bearing fault diagnosis is to select a suitable resonance frequency band, so as to filter out interference components to the maximum extent and retain fault information in the resonance band. Kurtogram algorithm can locate the resonance frequency band well, which has been widely researched and applied in recent years, and has produced many derivative algorithms. The statistical indicators used by these methods to identify frequency band features are divided into time domain indicators and frequency domain indicators. Time domain indicators are more sensitive to a single accidental impact components, while frequency domain indicators are easily affected by harmonics in the time domain, that is, single or several frequency extremes in the frequency domain. In order to overcome the impact of non-periodic transient impulse components and modulation harmonic components, this article proposes a new method. This method uses wavelet packet transform (WPT) to divide the frequency band plane, and adopts 3 iterations 1.5-dimensional spectrum (1.5D spectrum) method, which can eliminate the impulse interference that has no coupling relationship in the time domain and frequency domain. Based on the above process, the $K_{I-1.5D}$gram method is constructed, which can realize more accurate positioning of the fault information. Finally, through simulated and experimental analysis, the effectiveness of the proposed method is verified.

INDEX TERMS Bearing diagnosis, kurtogram, WPT, iterative 1.5D spectrum.

I. INTRODUCTION

As the joint of rotating machinery, rolling bearing is one of the most widely used parts in rotating machinery, with high failure rate and large life span. Carrying out rolling bearing condition monitoring and fault diagnosis research is of great significance for evaluating the operating status of rotating machinery and ensuring the safe and stable operation of the equipment [1]–[3]. For bearing failure analysis, many scholars have proposed effective signal processing methods, and the representative one is the Kurtogram.

Antoni and Randall [4] and Antoni [5] uses tree filter banks or short-time Fourier transform (STFT) to segment the frequency band plane, and then uses kurtosis index to evaluate the impulse information components in the sub-band signal. By this method, the optimal filtering frequency band can be selected, and the fault characteristic frequency can be extracted by further envelope spectrum (ES) analysis of the filtered signal. Since then, many scholars have proposed improved methods to overcome the shortcomings of kurtogram, and obtained many kurtogram derivative algorithms. Notably, the improvements of these kurtogram derivative algorithms are mainly concentrated in two aspects.

On the one hand, it is to ensure the compactness and sparsity of the filter design as much as possible, and the frequency band plane division is more reasonable, so as to maximize the fault information in a relatively complete sub-band. Lei *et al.* [6] introduced the wavelet packet transform (WPT) into the Kurtogram algorithm, replacing the STFT and tree filter bank in the original algorithm as a frequency band segmentation method. On the basis of Lei, Wang *et al.* [7] introduced the dual complex wavelet transform to the improvement of Kurtogram, and constructed the sub-band average kurtosis to replace the original time domain kurtosis. Wang and Tsui [8] applied dynamic Bayes to the optimization of WPT parameters, which can more accurately locate the

The associate editor coordinating the review of this manuscript and approving it for publication was Filbert Juwono.

center frequency and bandwidth, thereby achieving more accurate fault feature extraction. Qin *et al.* [9] constructed an improved Morlet wavelet that strictly satisfies the allowable conditions, which is very helpful for sparsely separating signal components. By using the improved Morlet wavelet dictionary and Fourier dictionary, transient components can be extracted by solving the sparse problem. And they use an improved kurtosis calculation method as a band positioning indicator. Gao *et al.* [10] constructed a new Kurtogram algorithm using Morlet wavelet filtering and alpha-stable distribution model, and used simulations and experiments to show the stability of the method against non-Gaussian features of gear faults. Xu *et al.* [11] proposed an adaptive Kurtogram method, which uses a step statistical filter to estimate and divide the effective modal components in the spectrum to replace the kurtosis calculation process.

On the other hand, it is necessary to design statistical indicators with specific sensitivity to fault information, so as to ensure the ability to identify fault characteristic sub-bands. The drawback of the kurtosis index is that it is too sensitive to occasional impacts and strong Gaussian noise in the time domain. To solve this problem, Barszcz and Jablonski [12] proposed a Protrugram method, which replaces the time domain kurtosis by calculating envelope spectral kurtosis. In the case of compound faults of bearing and gear meshing, Kurtogram method is difficult to distinguish the fault factors in the resonance frequency band. To solve this problem, Wang *et al.* [13] proposed a method combining spectral kurtosis and MRgram to isolate compound faults of bearing and gear. Moshrefzadeh and Fasana [14] proposed an Autogram method, which uses square envelope unbiased autocorrelation instead of time domain signals. Through this operation, the uncorrelated interference components can be discarded. Bao *et al.* [15] constructed a new index named envelope spectrum L-kurtosis. This index can suppress shock interference and harmonic interference in the time domain, making periodic fault components more specific. In order to solve the problem that it is difficult to extract the weak pulses masked by strong background noise in the fault diagnosis of rolling bearings, Li *et al.* [16] proposed an enhanced fault detection method based on the cyclic statistical characteristics of defective bearing vibration signals, combined with sparse code shrinkage denoising and fast spectral correlation. Furthermore, Antoni *et al.* [17] introduced entropy into the improvement of Kurtogram. By calculating the square envelope (SE) entropy in the time domain, the square envelope spectrum (SES) entropy in the frequency domain, and the combination of the two indicators, SE infogram, SES infogram and SE1/2/SES1/2 infogram were constructed respectively. Subsequently, many scholars conducted research on the application and improvement of infogram. Feng *et al.* [18] extended the infogram method to the fault diagnosis of planetary gearboxes. Li *et al.* [19] proposed a multi-scale clustering gray infogram by using multi-scale clustering to combine two negative entropies in a gray method. In order to solve the instability of Shannon entropy, Xu *et al.* [20] proposed the multiscale fractional order entropy (MSFE). With the help of MSFE infogram, the complexity and nonlinear characteristics of vibration signals can be evaluated by quantifying the spectral entropy on a series of scales in the fractional domain.

These studies improve the compactness of band segmentation and the accuracy of band selection to a certain extent. However, when dealing with extreme signals, such as when the processing signal contains non-periodic transient impulse components and modulation harmonic components, the processing capability of the algorithm faces challenges. Aiming at this problem, this article proposes an iterative 1.5-dimensional spectral kurtosis method, which can suppress the components that do not have a coupling relationship in the signal and avoid the influence of these components on the statistical feature indicators, thereby improving the accuracy of frequency band selection.

The outline of this article is as follows. Section 2 reviews the typical Kurtogram construction method and its limitations in dealing with non-periodic transient impulse components and modulation harmonic components. Section 3 introduces the iterative 1.5D spectral kurtosis construction method and its superiority in signal periodic feature extraction. two sets of experimental data are adopted, which respectively verify the effectiveness of the proposed method. Section 4 verifies the effectiveness of the proposed method with the aid of two sets of typical experimental data.

II. REVIEW OF KURTOGRAM AND ANALYSIS OF ITS LIMITATIONS

A. CONSTRUCTION METHOD OF KURTOGRAM BASED ON WPT

In this study, the WPT-based sub-band construction method proposed in 2011 was discussed as a typical Kurtogram method [7]. The construction process of this method and its limitations in dealing with signals with uncoupled interference are reviewed.

For a non-stationary signal $x(t)$, suppose its response is $y(t)$, which can be expressed as Equation (1).

$$y(t) = \int_{-\infty}^{+\infty} e^{2\pi fjt} H(t,f)\, dx(f) \tag{1}$$

where $H(t,f)$ is the transfer function and $dx(f)$ is the spectral increment.

The second-order spectral moment of $y(t)$ can be defined as Equation 2.

$$\begin{aligned} S_{2\mathrm{ny}}(t,f) &= E\left\{\left|H(t,f)\, dX(f)^{2n}\right|\right\}/df \\ &= |H(t,f)|^{2n} \cdot S_{2nx} \end{aligned} \tag{2}$$

When $2n = 2$, Equation 2 can be abbreviated as Equation 3:

$$S_{2\mathrm{y}}(t,f) = E\left\{\left|H(t,f)^2\right|\right\} \cdot \sigma_{\mathrm{x}}^2 \tag{3}$$

Further, The fourth-order spectral cumulant can be defined as Equation 4:

$$C_{4\mathrm{y}}(f) = S_{4y}(f) - 2S_{2y}^2(f) \tag{4}$$

The fourth-order normalized cumulant can be used to define the spectral kurtosis, as shown in Equation 5:

$$K_x = \frac{C_{4y}(f)}{S_{2y}^2(f)} = \frac{S_{4y}(f) - 2S_{2y}^2(f)}{S_{2y}^2(f)} = \frac{S_{4y}(f)}{S_{2y}^2(f)} - 2 = \frac{\langle |H(t,f)|^4 \rangle}{\langle |H(t,f)|^2 \rangle^2} - 2 \tag{5}$$

WPT can continuously decompose the high-frequency and low-frequency components of the signal at the same time, and can adaptively determine the resolution of different frequency bands, which greatly improves the signal time-frequency local analysis ability, and is widely used. The wavelet packet transformation process can be expressed by Equation 6.

WPT can continuously decompose the high-frequency and low-frequency components of the signal at the same time, and can adaptively determine the resolution of different frequency bands, which greatly improves the signal time-frequency local analysis ability. The wavelet packet transformation process can be expressed by Equation 6.

$$\begin{cases} x_{i,j} = \sqrt{2}\sum_{n=0}^{K} L_n x_{i-1,j+n} \\ x_{i,j+1} = \sqrt{2}\sum_{n=0}^{K} G_n x_{i-1,j+n} \end{cases} \tag{6}$$

where $x_{i,j}$ represents the j-th sub-band signal of the i-th layer ($i = 1, 2, \ldots, I$ where I is the number of decomposition levels; $j = 1, 2, \ldots, J$, where I is the number of decomposition levels, J is the number of signals of the corresponding layer, and $J = 2^I$); L_n and G_n are the low-pass filter and high-pass filter of the wavelet packet, respectively.

The signal is decomposed by wavelet packet, and then the spectral kurtosis value of each sub-band signal is calculated separately, and the kurtosis distribution of the entire frequency band plane can be obtained, as shown in Figure 1.

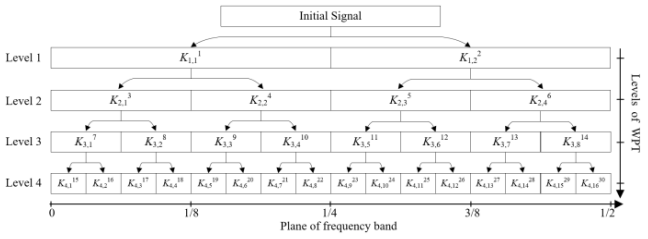

FIGURE 1. Kurtogram based on WPT.

B. LIMITATIONS OF THE ALGORITHM

The limitations of the Kurtogram algorithm are mainly caused by its statistical characteristics. As we all know, kurtosis can capture transient information, so it can detect fault impact information. However, in some cases, some abnormal shock components will affect the recognition of the kurtosis index. Kurtosis index is very sensitive to non-periodic transient impulse components. Abnormal vibration and accidental shock of equipment will cause non-periodic transient impulse components, which will lead to the failure of kurtosis index in time domain. In addition, the harmonic components of vibration signal will form non-periodic transient components in envelope spectrum (frequency domain), which will lead to the failure of kurtosis index of frequency domain. In order to illustrate this point, a simulated signal defined as Equation (7) is used for analysis. The simulated signal consists of four parts: y_1 represents periodic impulse components, y_2 represents non-periodic transient impuls components, y_3 represents modulation harmonic components, $n(t)$ represents a certain degree of noise, and Y is the composite signal of four components.

$$\begin{cases} y_1 = \sum_{i=1}^{n} A e^{-\xi[t-q_i(t)/f_{outer}]^2} \cdot \sin(2\pi f_o t) \\ y_2 = A_1 e^{[-b_1\times(t-t_1)]} \cdot \sin[2\pi f_1 \cdot (t-t_1)] \\ \qquad + A_2 e^{[-b_2\times(t-t_2)]} \cdot \sin[2\pi f_2 \cdot (t-t_2)] \\ y_3 = A_3 \cdot \sin(2\pi f_{mesh} t + \beta_1)(1 + A_4 \sin(2\pi f_h t + \beta_2)) \\ Y = y_1 + y_2 + y_3 + n(t) \end{cases} \tag{7}$$

where A $=$ 2 is the amplitude of the periodic impulse components, $A_1 = 3$ and $A_2 = 6$ are the amplitudes of the non-periodic transient impulse components, $A_3 = A_4 = 0.6$ are the amplitudes of the modulation harmonic components. ξ is the damping ratio, f_o is the natural frequency of the system, f_{outer} is the characteristic frequency of the periodic impulse components. $b_1 = 260$, $b_2 = 360$, $t_1 = 0.2$, $t_2 = 0.3$, and $f_1 = f_2 = 3600$Hz are damping parameters, time parameters, and natural frequencies of non-periodic transient impuls components, respectively. $n(t)$ is the noise (SNR$= -12$dB). The parameters of the simulated signal are listed in TABLE 1.

TABLE 1. Parameters of the simulated signal.

Parameter type	Parameter values
Sampling frequency (Hz)	8192
Sampling points (Hz)	8192
Natural frequency f_o (Hz)	2100
Natural frequency $f_1 = f_2$ (Hz)	3600
Carrier frequency f_{mesh}	360
Modulation frequency f_h	15
Fault frequency f_{outer} (Hz)	50

Figure 2(a) is the time domain waveform of periodic impulse components, Figure 2(b) is the time domain waveform of non-periodic transient impulse components, Figure 2(c) is the time domain waveform of modulation harmonic components, and Figure 2(d) is the time domain waveform of noise components, Figure 2(e) is the composite signal of four components, Figure 2(f) is the spectrum of Figure 2(e). It can be found from Figure 2(f) that the periodic impulse components information in the time domain is mainly concentrated near the resonance frequency band of 2100Hz, and the modulated harmonic components have a large amplitude in the spectrum (360Hz), so it can be

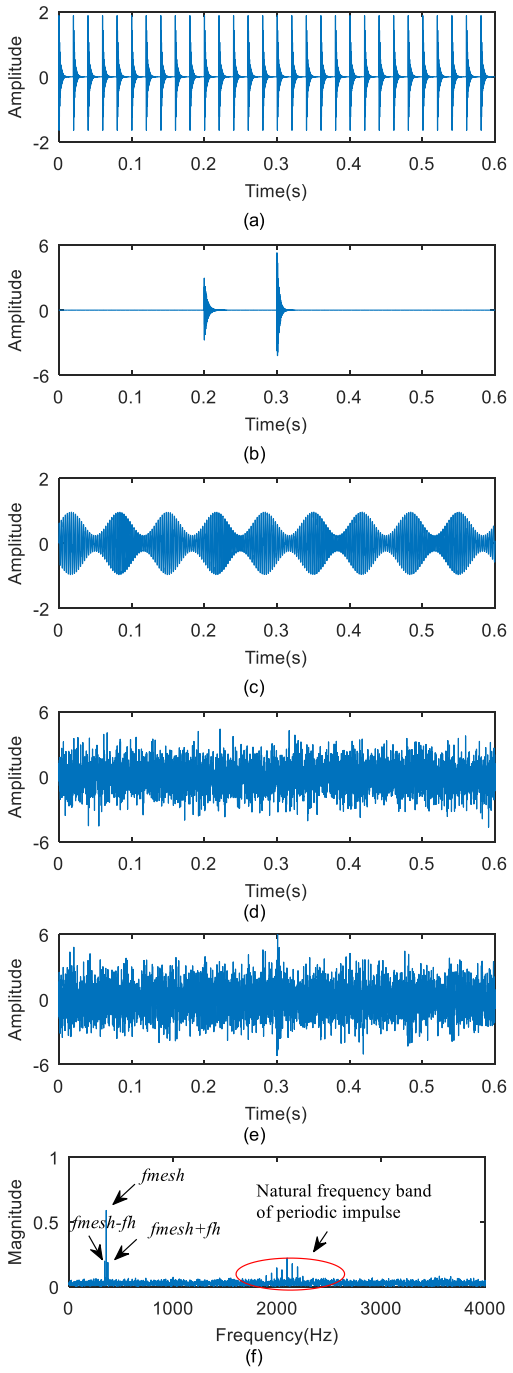

FIGURE 2. (a) Time domain waveform of periodic impulse components (y_1), (b) time domain waveform of non-periodic transient impulse components (y_2), (c) time domain waveform of modulation harmonic components (y_3), (d) time domain waveform of noise components ($n(t)$), (e) composite signal of four components (Y), and (f) spectrum of (e).

considered that the modulated harmonic is a non-periodic transient impulse in the frequency domain.

Figure 3 is the envelope spectrum of the composite signal in Figure 2(e). It can be seen from Figure 3 that the spectral line of harmonic frequency components are prominent, while the spectral lines of fault characteristic frequency and its multiple frequency components are almost covered.

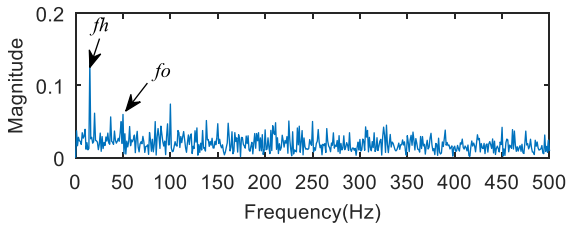

FIGURE 3. Envelope spectrum of the composite signal (Y).

The spectral kurtosis defined in time domain (K_{se}gram) and spectral kurtosis defined in frequency domain (K_{ses}gram) are applied to the composite signal components (Y) respectively. The results are shown in Figure 4. It is found from Figure 4(a) that the optimal frequency band found by K_{se}gram is in the 15th sub-band of the fourth layer, which is close to the frequency of the non-periodic transient impulse components (3600Hz), while the optimal frequency band found by the s algorithm is in the second sub-band of the fourth layer, which is close to the carrier frequency of the modulation harmonic components (360Hz). The corresponding sub-bands are analyzed in time domain, and the results are shown in Figure 4(c) and Figure 4(d) respectively. The non-periodic impulse components and the modulated harmonic components are obtained.

The results show that neither the K_{se}gram algorithm defined in time domain nor the K_{ses}gram algorithm defined in frequency domain can accurately locate the sub-band of periodic impulse components.

III. ITERATIVE 1.5D SPECTRAL KURTOSIS ALGORITHM

In order to solve the non-periodic transient impulse interference in the time domain and the harmonic singular line interference in the frequency domain at the same time, an iterative 1.5D spectral kurtosis processing method is proposed.

A. TEAGER ENERGY OPERATOR

Teager energy operator (TEO) is a nonlinear operator that can strengthen the transient impulse components in the signal, and capture the characteristic components related to the fault impulse in the signal. For a signal $x(t)$, its TEO(φ) can be expressed as follow:

$$\varphi[x(t)] = [\dot{x}(t)]^2 - x(t)\ddot{x}(t) \tag{8}$$

where $\dot{x}(t)$ and $\ddot{x}(t)$ are the first and second order differentials of $x(t)$, respectively.

For an undamped vibration system composed of a mass of m block and a spring of stiffness k, the following differential equation can be established.

$$m\ddot{x}(t) + kx(t) = 0 \tag{9}$$

where $x(t)$ can be regarded as the displacement of the mass block, and $\ddot{x}(t)$ can be regarded as the acceleration of the mass block, then the solution of the differential equation can be expressed as Equation (10).

$$x(t) = A\cos(\omega t + \varphi) \tag{10}$$

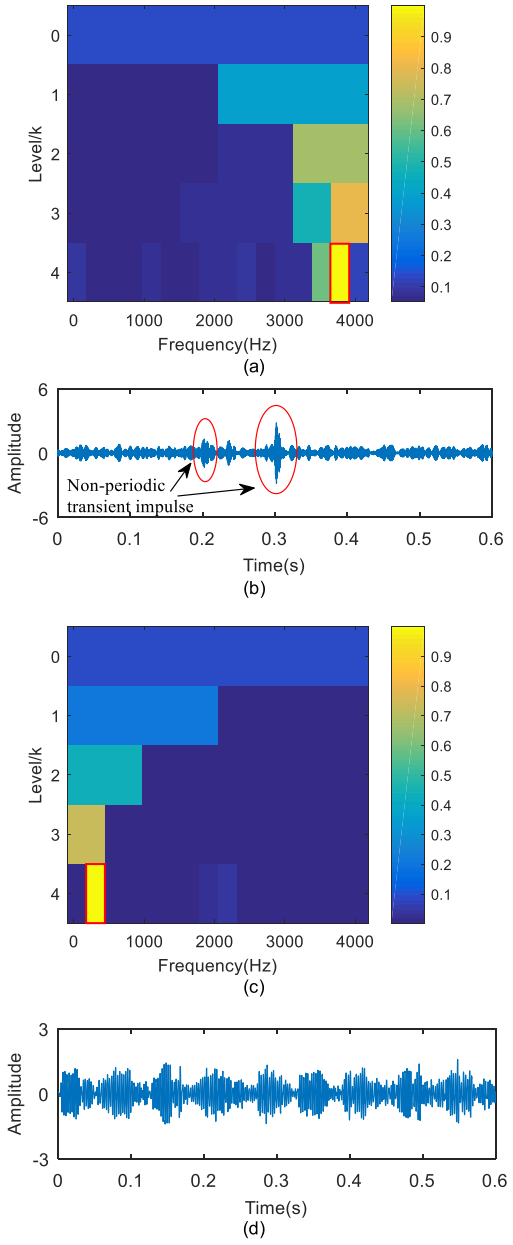

FIGURE 4. (a) K_{se}gram of the simulated signal (Y), (b) time domain waveform of 15th sub-band of the fourth layer, (c) K_{ses}gram of the simulated signal (Y), (d) time domain waveform of second sub-band of the fourth layer.

Correspondingly, the first-order differential can be expressed by Equation (11), and the second-order differential can be expressed by Equation (12).

$$\dot{x}(t) = -A\omega \sin(\omega t + \varphi) \tag{11}$$

$$\ddot{x}(t) = -A\omega^2 \cos(\omega t + \varphi) \tag{12}$$

where A is amplitude, $\omega = (k/m)^{1/2}$ is natural frequency, and φ is initial phase. At any time, the mechanical energy of the vibration system can be expressed as the sum of the spring potential energy and the mass kinetic energy, which can be expressed in terms of Equation (13) as follows:

$$E = \frac{1}{2}k[x(t)]^2 + \frac{1}{2}m[\dot{x}(t)]^2 \tag{13}$$

Further, Equation (14) can be obtained as follows:

$$E = \frac{1}{2}mA^2\omega^2 \tag{14}$$

Equation (14) establishes the relationship between the total instantaneous energy of vibration and the amplitude and frequency of vibration. Then the TEO (φ) defined in Equation (8) is applied to the simple harmonic oscillation, which can be expressed as Equation (15).

$$\varphi[x(t)] = \varphi[A\cos(\omega t + \varphi)] = A^2\omega^2 \tag{15}$$

Equation (15) shows that TEO is the product of the square of the amplitude and the square of the instantaneous frequency. Compared with the traditional energy definition, the relationship between TEO calculation value and frequency can be improved.

B. ITERATIVE 1.5D SPECTRAL KURTOSIS

The diagonal slice of the third-order cumulant $R_{3x}(\tau_1, \tau_2)(\tau_1 = \tau_2 = \tau)$ of the stationary signal can be defined as follows [21], [22]:

For a signal $x(t)$, the diagonal slice of the third-order cumulant $R_{3x}(\tau_1, \tau_2)(\tau_1 = \tau_2 = \tau)$ can be expressed by Equation 16.

$$R_{3x}(\tau, \tau) = E\{x(t)\,x(t+\tau)\,x(t-\tau)\} \tag{16}$$

where $E\{\cdot\}$ represents mathematical expectation.

The 1.5D spectrum of the original signal $x(t)$ can be obtained by performing Fourier transform on the three diagonal slices.

$$B(\omega) = \int_{-\infty}^{\infty} R_{3x}(\tau, \tau)\, e^{-j\omega\tau} d\tau \tag{17}$$

According to demodulation of the time domain signal with TEO, instead of envelope demodulation of the original time domain signal, $B^1(\omega)$ can be obtained as follows:

The TEO (φ) is used to replace the original signal $x(t)$, and the 1.5D spectrum of the energy operator is obtained as shown in Equation 18.

$$B^1(\omega) = \int_{-\infty}^{\infty} W_{3\varphi}(\tau, \tau)\, e^{-j\omega\tau} d\tau \tag{18}$$

$B^1(\omega)$ is regarded as a discrete sequence, and then 1.5D spectrum analysis is carried out to obtain the second iteration spectrum. In the same way, $B^2(t)$ is regarded as a discrete sequence, and then the 1.5D spectrum analysis is carried out to obtain the third iteration spectrum.

$$B^2(t) = \int_{-\infty}^{\infty} R_{3B^1}(\omega, \omega)\, e^{-j\omega\tau} d\omega \tag{19}$$

$$B^3(\omega) = \int_{-\infty}^{\infty} R_{3B^2}(\tau, \tau)\, e^{-j\omega\tau} d\tau \tag{20}$$

The spectral distance of the three iteration spectrum discrete sequence is calculated and brought into Equation (5), and the spectral kurtosis value $K^3_{\text{I-1.5D}}$ of the three iteration spectral distance is obtained.

$$K_{\text{I-1.5D}} = \frac{\left\langle \left| B^3(t,f) \right|^4 \right\rangle}{\left\langle \left| B^3(t,f) \right|^2 \right\rangle^2} - 2 \tag{21}$$

Each sub-band of the wavelet packet is operated separately to obtain the 1.5D spectral kurtosis distribution in the frequency plane, as shown in Figure 4. Thus, the optimal sub-band can be selected, that is, the sub-band with the most fault information.

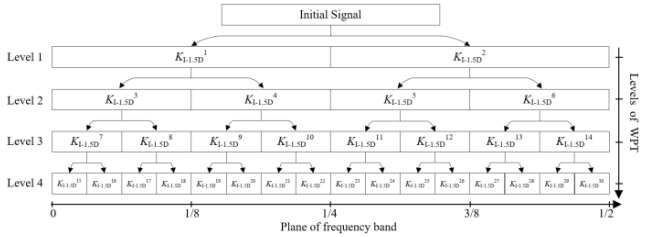

FIGURE 5. Paving of $K_{I-1.5D}$gram.

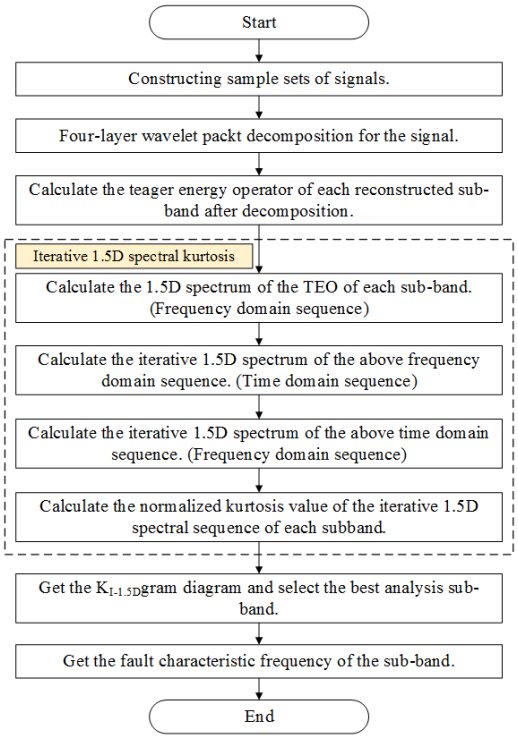

FIGURE 6. Flow chart of the proposed algorithm.

The steps of the proposed method are shown in Figure 6 as follows:

First, the time domain sequence of the collected signal is decomposed by 4-layer WPT. Each sub-band signal after decomposition is reconstructed, and the TEO of the time domain sequence of the reconstructed signal is calculated. This step is to enhance the impact characteristics in the signal. Then, the TEO of each reconstructed sub-band is computed by iterative 1.5D spectral kurtosis. The specific process is: calculate the 1.5D spectrum for the time domain sequence to obtain the frequency domain sequence, perform the iterative 1.5D spectrum operation on the frequency domain sequence to restore the time sequence, and then iterate the 1.5D spectrum on the time sequence to obtain the frequency domain sequence. The iterative 1.5D spectrum can suppress the components which have no coupling relationship in the time domain and frequency domain sequences. Finally, the normalized kurtosis values of the iterated 1.5D spectral sequences of all subbands are calculated and the $K_{I-1.5D}$gram is obtained, so that the optimal subband can be selected. By analyzing the optimal subband, the fault characteristic frequency can be obtained.

C. SUPERIORITY OF ITERATIVE 1.5D SPECTRAL KURTOSIS

The 1.5D spectrum has three characteristics: one is to make the spectrum energy incline to the low-frequency part, so as to capture the fault characteristic frequency; the second is to suppress the Gaussian noise to make the noise spectrum line tend to zero; the third is to suppress the spectrum line without coupling relationship, which can avoid the interference of single harmonic spectrum line in frequency domain.

(1) For a real harmonic signal $x(t)$ with a mean value of 0 and a fundamental frequency ω_0, when there are frequencies $|\omega_m|$ and $|\omega_m|$ and $|\omega_m| < |\omega_l|$, then:

$$\begin{cases} B(\omega_m) > B(\omega_l), \\ \omega_m = m\omega_0, \quad m = \pm 1, \ \pm 2, \ldots, \ \pm n, \\ \omega_l = l\omega_0, \quad l = \pm 1, \ \pm 2, \ldots, \ \pm n. \end{cases}$$

This characteristic shows that the signal energy in the 1.5D spectrum tends to lower harmonic frequencies, especially the fundamental frequency, which enhances the low-frequency components in the signal and makes them easy to extract.

(2) Assuming that n is Gaussian white noise with a mean value of 0, then its 1.5D spectrum $B(\omega) = 0$.

$$B(\omega) = \int_{-\infty}^{\infty} R_{3n(t)}(\tau, \tau) e^{-j\omega\tau} d\tau = 0$$

This means that the 1.5D spectrum can suppress Gaussian noise.

(3) For a harmonic signal $x(t)$ containing three frequency components (ω_1, ω_2, and ω_3), and $\omega_1 > \omega_2 > \omega_3$. If the three frequency components have no coupling relationship, that is, $\omega_1 \neq \omega_2 + \omega_3$, then their 1.5D spectrums tend to 0 ($B(\omega_1) = 0$, $B(\omega_2) = 0$, and $B(\omega_3) = 0$). If the three frequency components have a coupling relationship, that is, $\omega_1 = \omega_2 + \omega_3$, then $B(\omega_1) \neq 0$, $B(\omega_2) \neq 0$, and $B(\omega_3) \neq 0$. The above process shows that the 1.5D spectrum can suppress the non-coupling components in the signal and enhance the coupling components, and the harmonics in the fault pulse have a coupling relationship. In other words, the 1.5D spectrum can enhance the fault characteristics in the frequency domain.

Because of the three characteristics of 1.5D spectrum, the accidental interference and Gaussian noise without coupling relationship are eliminated in the time domain and frequency domain during the three iterations.

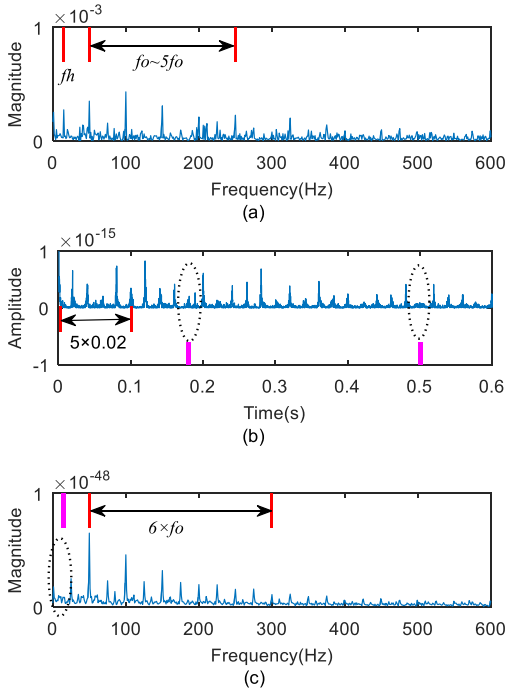

FIGURE 7. (a) 1.5D spectrum ($B^1(\omega)$) of the TEO of the original signal (Y), (b) second iteration 1.5D spectrum ($B^2(t)$), (c) third iteration 1.5D spectrum ($B^3(\omega)$).

In order to illustrate the process of iterating 1.5D spectrum and its suppression effect on uncoupled components in time and frequency domain, the simulated signal defined in Equation (7) is analyzed. The teager energy operator of the composite signal (Y) is calculated, and then the 1.5D spectrum operation is performed on the discrete sequence. Figure 7(a) is the result. Compared with the envelope spectrum in Figure 3, it can be found that the 1.5D spectrum can suppress the noise better, and the fault characteristic frequency with coupling relationship can be obtained, and the harmonic components are suppressed to a certain extent. Then perform the second iteration on the 1.5D spectrum, the result is shown in Figure 7(b). It can be found that in the time domain waveform, the periodic impulse components with the coupling relationship are more prominent, but the non-periodic transient impulse components without the coupling relationship are suppressed. Similarly, the third iteration 1.5D spectrum is performed again, and the result is shown in Figure 7(c). The results show that the non-periodic transient impulse components and harmonic components that do not have a coupling relationship in the time and frequency domains have been eliminated, and only the periodic impulse components with the coupling relationship have been retained.

The above method is used to construct an iterative 1.5D spectral kurtosis index, which is applied to the selection of

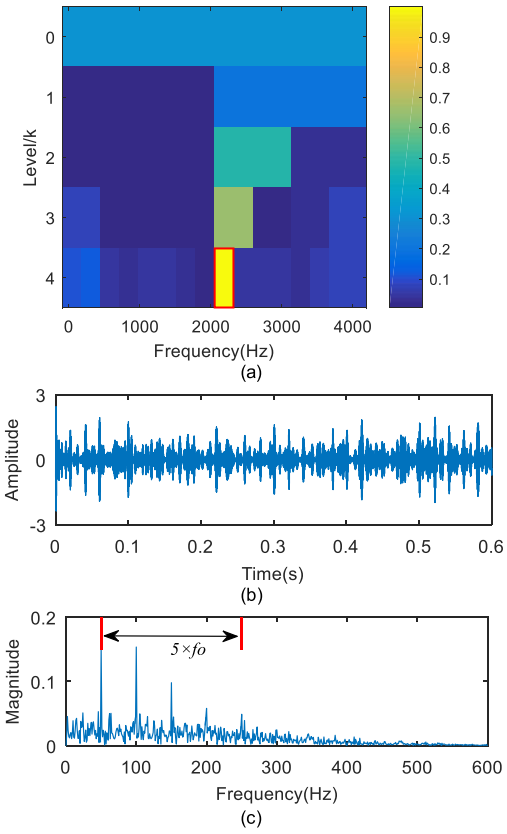

FIGURE 8. (a) $K_{I-1.5D}$gram of the original signal (Y), (b) time domain waveform of ninth sub-band of the fourth layer, (c) envelope spectrum of (b).

optimal sub-bands. Firstly, the original signal is decomposed into four layers of wavelet packets, and then the iterative 1.5D spectral kurtosis value of each wavelet sub-band is calculated. The results are shown in Figure 8. It can be found from Figure 8(a) that the optimal sub-band is in the ninth sub-band of the fourth layer, which coincides with the frequency band where the periodic impulse components is located (2100Hz). Furthermore, periodic impulse characteristics can be obtained in the time domain, and fault characteristic frequencies can be obtained in the envelope spectrum.

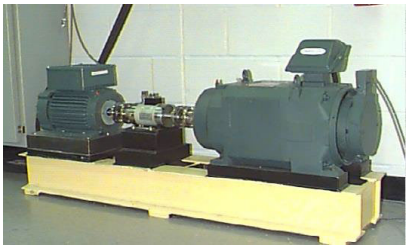

FIGURE 9. Bearing fault experimental equipment of CWRU.

IV. EXPERIMENTAL ANALYSIS

A. CASE 1: EXPERIMENTAL DATA WITH NON-PERIODIC TRANSIENT IMPULSE COMPONENTS

In order to verify the effectiveness of the proposed method, the bearing vibration signal data of CWRU was analyzed.

TABLE 2. Parameters of the simulated signal.

Parameter type (LYC6205E)	Parameter values
Pitch Diameter (mm)	28.5
Ball Diameter (mm)	6.7
Number of Balls	8
Contact Angle (°)	0

TABLE 3. Theoretical fault characteristic frequency of bearings.

Type of fault	Parameter values
Outer ring fault	88
Inner ring fault	143
Rolling elment fault	115

The experimental equipment is shown in Figure 9. The bearing model is JEMSKF6023-2RS, and the relatively early fault data (0.007 inch) are selected for analysis. The sampling frequency is 12000 Hz and the spindle speed is 1730 rpm. The structural parameters of the bearings used are shown in TABLE 2. Based on the bearing parameters, the theoretical fault characteristic frequency of the bearings shown in TABLE 3 can be calculated.

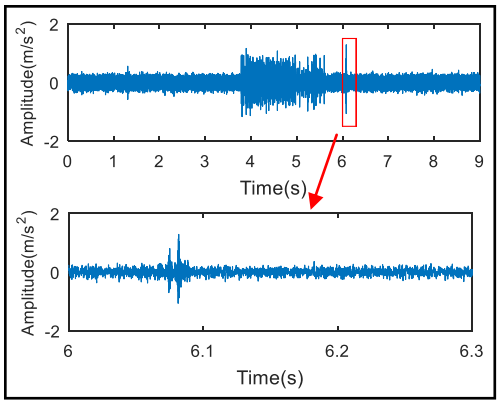

FIGURE 10. Time domain waveform of the experimental signal.

The time domain waveform of the experimental signal is shown in Figure 10. It can be seen that the experimental data contains obvious impact interference, and part of the data (6-6.3s) is selected for analysis.

The above-mentioned experimental signal is analyzed by the traditional Kurtogram method defined in the time domain (K_{se}gram), and the results are shown in Figure 11. From Figure 11(a), it can be found that the determined optimal sub-band is the ninth sub-band of the fourth layer. By analyzing this sub-band, a significant impact interference can be found from the time domain (Figure 11(b)). This shows that the Kurtogram method defined by the time domain kurtosis has poor ability to deal with accidental impact interference and is susceptible to this type of interference.

The $K_{I-1.5D}$gram defined by the iterative 1.5D spectral kurtosis mentioned in this article is used to process the above experimental signals, and the results are shown in Figure 12. From Figure 12(a), it is found that the twelfth sub-band of the

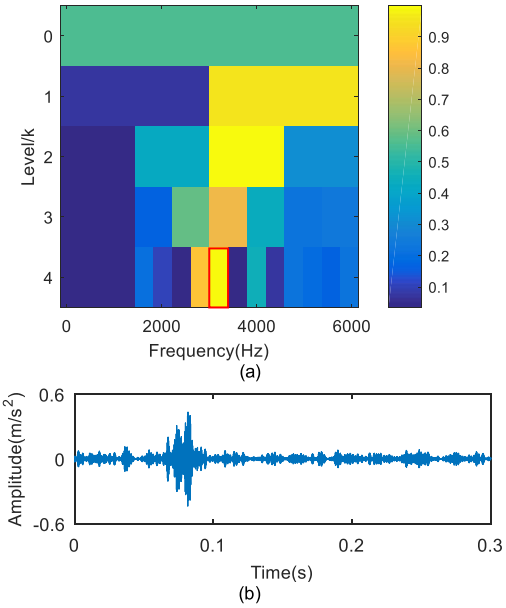

FIGURE 11. (a) K_{se}gram of the experimental signal, (b) time domain waveform of ninth sub-band of the fourth layer.

fourth layer is the optimal frequency band. By analyzing this sub-band, more obvious impulse information can be obtained from the time domain waveform (Figure 12(b)), and there are obvious fault features in the envelope spectrum.

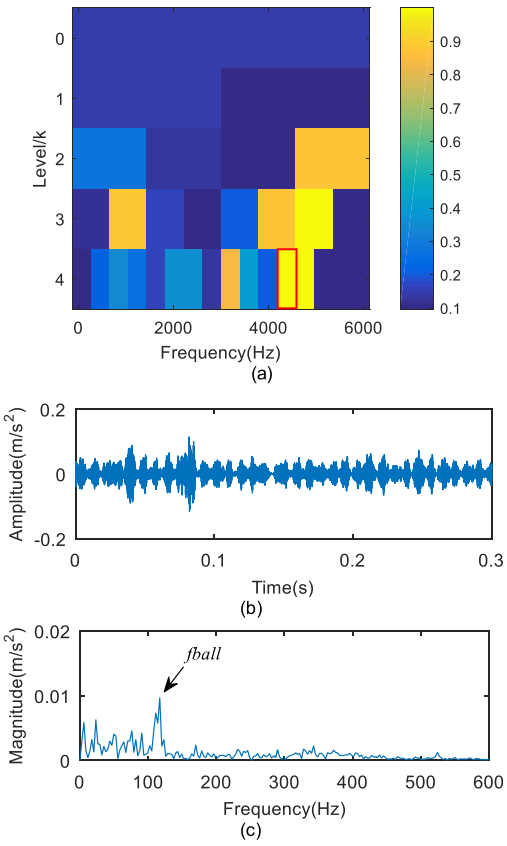

FIGURE 12. (a) $K_{I-1.5D}$gram of the experimental signal, (b) time domain waveform of twelfth sub-band of the fourth layer, (c) envelope spectrum of (b).

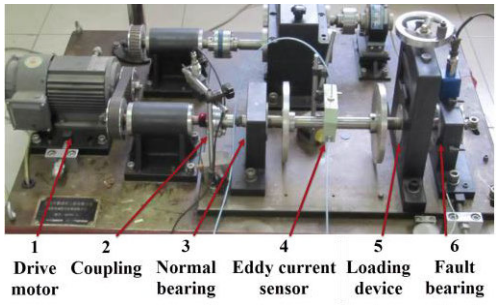

FIGURE 13. Bearing fault experimental equipment of QPZZ-II.

B. CASE 2: EXPERIMENTAL DATA WITH MODULATION HARMONIC COMPONENTS

In order to further verify the effectiveness of the proposed method, the data of the QPZZ-II rolling bearing failure test bench is used for analysis. The structure of the experimental platform is shown in Figure 13. The test bench uses a single drive motor as the power source, and the belt drives the shaft for synchronous rotation. EDM is used to cause local damage to the outer ring of the bearing (the fault is a groove with a depth of 1.5mm and a width of 0.2mm), and the faulty bearing is placed in the bearing seat. The eddy current sensor is used to measure the vibration displacement in the horizontal and numerical directions of the rotating shaft, and the vibration acceleration sensor is used to measure the vibration of the bearing seat. In this experiment, the speed is set to 1440rpm, the rotation frequency of the shaft is 24Hz, and the sampling frequency is 12800Hz. The bearing signal is N205 cylindrical roller bearing, its structural parameters are shown in TABLE 4, and the fault characteristic frequency obtained by theoretical calculation is shown in TABLE 5.

TABLE 4. Parameters of the simulated signal.

Parameter type (N205)	Parameter values
Pitch Diameter (mm)	38.5
Ball Diameter (mm)	7.5
Number of Balls	12
Contact Angle (°)	0

The data of the eddy current sensor is used for analysis. The time domain waveform is shown in Figure 14. It can be found that due to the imbalance of the rotating shaft, there is a large low frequency in the displacement signal, but the high frequency vibration characteristics are not obvious. Envelope spectrum analysis is directly performed on the original signal. Obvious spectral transition lines can be extracted from the envelope spectrum, but the fault characteristic frequency cannot be extracted.

Kurtogram algorithm defined by the frequency domain (K_{ses}gram) is used to analyze the experimental signal. It can be seen that the optimal frequency band is the first sub-band of the fourth layer (Figure 15(a)). From the time domain waveform (Figure 15(b)) and envelope spectrum (Figure 15(c)), it can be found that the sub-band corresponds to the frequency band where the harmonic components of the frequency conversion are located, and the fault characteristic information cannot be extracted.

TABLE 5. Theoretical fault characteristic frequency of bearings.

Type of fault	Parameter values
Outer ring fault	116
Inner ring fault	172
Rolling elment fault	123

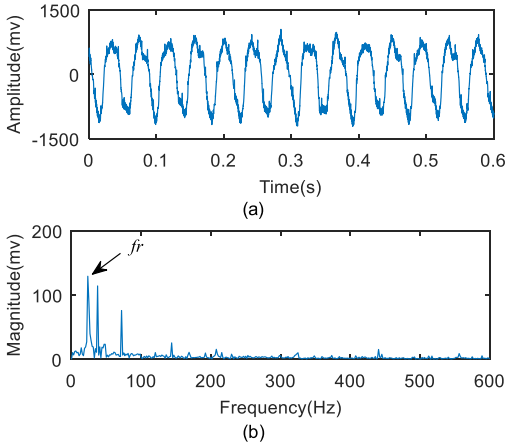

FIGURE 14. (a) Time domain waveform of the experimental signal, (b) envelope spectrum of (a).

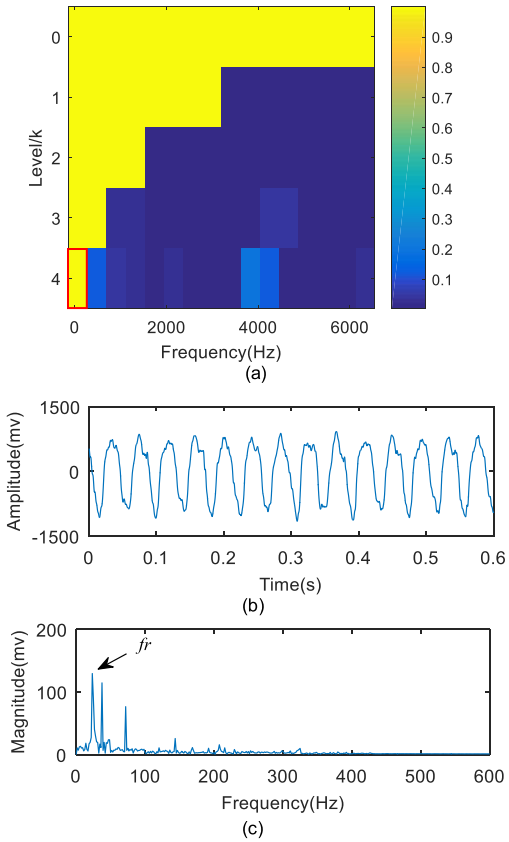

FIGURE 15. (a) K_{ses}gram of the experimental signal, (b) time domain waveform of first sub-band of the fourth layer, (c) envelope spectrum of (b).

The method proposed in this article is used to analyze the original experimental signal. The result is shown in Figure 16. From Figure 16(a), it can be found that the optimal filtering frequency band located is the sixth sub-band

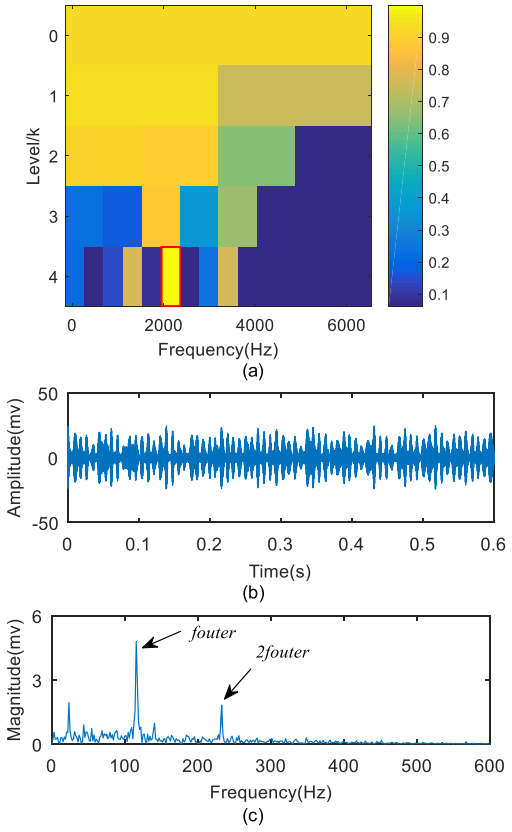

FIGURE 16. (a) $K_{I-1.5D}$gram of the experimental signal, (b) time domain waveform of sixth sub-band of the fourth layer, (c) envelope spectrum of (b).

of the fourth layer. The time domain analysis and envelope spectrum analysis are performed on this sub-band, and the results are shown in Figure 16(b) and 16(c). The fault characteristic frequency and its multiplier components can be extracted, indicating the accuracy of the frequency band location of the proposed method.

V. CONCLUSION

In order to solve the feature recognition problem caused by the time domain statistical indicators being too sensitive to the non-periodic transient impulse components and the frequency domain statistical indicators being too sensitive to the modulation harmonic components, this article proposes an improved method based on iterative 1.5D spectrum. First, WPT is perform on the signal, and then the iterative 1.5D spectral kurtosis of the decomposed sub-bands is calculated to identify the best filtering frequency band. Through simulated and experimental analysis, it is verified that the proposed method can effectively suppress interference components that do not have a coupling relationship in the time domain and the frequency domain.

REFERENCES

[1] Y. Li, Y. Wei, K. Feng, X. Wang, and Z. Liu, "Fault diagnosis of rolling bearing under speed fluctuation condition based on Vold-Kalman filter and RCMFE," *IEEE Access*, vol. 6, pp. 37349–37360, 2018.

[2] L. Cui, Z. Jin, J. Huang, and H. Wang, "Fault severity classification and size estimation for ball bearings based on vibration mechanism," *IEEE Access*, vol. 7, pp. 56107–56116, 2019.

[3] Z. Huo, Y. Zhang, P. Francq, L. Shu, and J. Huang, "Incipient fault diagnosis of roller bearing using optimized wavelet transform based multi-speed vibration signatures," *IEEE Access*, vol. 5, pp. 19442–19456, 2017.

[4] J. Antoni and R. B. Randall, "The spectral kurtosis: Application to the vibratory surveillance and diagnostics of rotating machines," *Mech. Syst. Signal Process.*, vol. 20, no. 2, pp. 308–331, Feb. 2006.

[5] J. Antoni, "Fast computation of the kurtogram for the detection of transient faults," *Mech. Syst. Signal Process.*, vol. 21, no. 1, pp. 108–124, Jan. 2007.

[6] Y. Lei, J. Lin, Z. He, and Y. Zi, "Application of an improved kurtogram method for fault diagnosis of rolling element bearings," *Mech. Syst. Signal Process.*, vol. 25, no. 5, pp. 1738–1749, Jul. 2011.

[7] L. Wang, Z. Liu, and H. Cao, "Subband averaging kurtogram with dual-tree complex wavelet packet transform for rotating machinery fault diagnosis," *Mech. Syst. Signal Process.*, vol. 142, no. 2, pp. 1–21, Aug. 2020.

[8] D. Wang and K. Tsui, "Subband averaging kurtogram with dual-tree complex wavelet packet transform for rotating machinery fault diagnosis," *Mech. Syst. Signal Process.*, vol. 142, no. 2, pp. 1–21, Aug. 2020.

[9] Y. Qin, J. Zou, and F. Cao, "Adaptively detecting the transient feature of faulty wind turbine planetary gearboxes by the improved kurtosis and iterative thresholding algorithm," *IEEE Access*, vol. 6, pp. 14602–14612, 2018.

[10] M. Gao, G. Yu, and T. Wang, "Impulsive gear fault diagnosis using adaptive Morlet wavelet filter based on alpha-stable distribution and kurtogram," *IEEE Access*, vol. 7, pp. 72283–72296, 2019.

[11] Y. Xu, K. Zhang, C. Ma, L. Cui, and W. Tian, "Adaptive kurtogram and its applications in rolling bearing fault diagnosis," *Mech. Syst. Signal Process.*, vol. 130, pp. 87–107, Sep. 2019.

[12] T. Barszcz and A. JabŁoński, "A novel method for the optimal band selection for vibration signal demodulation and comparison with the kurtogram," *Mech. Syst. Signal Process.*, vol. 25, no. 1, pp. 431–451, Jan. 2011.

[13] T. Wang, F. Chu, Q. Han, and Y. Kong, "Compound faults detection in gearbox via meshing resonance and spectral kurtosis methods," *J. Sound Vib.*, vol. 392, pp. 367–381, Mar. 2017.

[14] A. Moshrefzadeh and A. Fasana, "The autogram: An effective approach for selecting the optimal demodulation band in rolling element bearings diagnosis," *Mech. Syst. Signal Process.*, vol. 105, pp. 294–318, May 2018.

[15] W. Bao, X. Tu, Y. Hu, and F. Li, "Envelope spectrum L-kurtosis and its application for fault detection of rolling element bearings," *IEEE Trans. Instrum. Meas.*, vol. 69, no. 5, pp. 1993–2002, May 2020.

[16] J. Li, Q. Yu, X. Wang, and Y. Zhang, "An enhanced rolling bearing fault detection method combining sparse code shrinkage denoising with fast spectral correlation," *ISA Trans.*, vol. 102, pp. 335–346, Jul. 2020.

[17] J. Antoni, "The infogram: Entropic evidence of the signature of repetitive transients," *Mech. Syst. Signal Process.*, vol. 74, pp. 73–79, Jun. 2016.

[18] Z. Feng, H. Ma, and M. J. Zuo, "Spectral negentropy based sidebands and demodulation analysis for planet bearing fault diagnosis," *J. Sound Vib.*, vol. 410, pp. 124–150, Dec. 2017.

[19] C. Li, D. Cabrera, J. V. de Oliveira, R.-V. Sanchez, M. Cerrada, and G. Zurita, "Extracting repetitive transients for rotating machinery diagnosis using multiscale clustered grey infogram," *Mech. Syst. Signal Process.*, vols. 76–77, pp. 157–173, Aug. 2016.

[20] X. Xu, Z. Qiao, and Y. Lei, "Repetitive transient extraction for machinery fault diagnosis using multiscale fractional order entropy infogram," *Mech. Syst. Signal Process.*, vol. 103, pp. 312–326, Mar. 2018.

[21] J. Cai and X. Li, "Gear fault diagnosis based on empirical mode decomposition and 1.5 dimension spectrum," *Shock Vib.*, vol. 2016, pp. 1–10, Jan. 2016.

[22] X. Yan and M. Jia, "Improved singular spectrum decomposition-based 1.5-dimensional energy spectrum for rotating machinery fault diagnosis," *J. Brazilian Soc. Mech. Sci. Eng.*, vol. 41, no. 1, p. 50, Jan. 2019.

XIONG ZHANG (Member, IEEE) was born in Hebei, China, in 1990. He received the Ph.D. degree from North China Electric Power University, China, in 2019. He is currently a Lecturer with the School of Mechanical Engineering, North China Electric Power University. His research interests include condition monitoring and fault diagnosis of power equipment.

SHUTING WAN was born in Shanxi, China, in 1971. He received the Ph.D. degree from North China Electric Power University, China, in 2006. He is currently a Professor with the School of Mechanical Engineering, North China Electric Power University. His research interests include condition monitoring and fault diagnosis of power equipment.

YULING HE (Member, IEEE) was born in Fujian, China, in 1984. He received the Ph.D. degree from North China Electric Power University, China, in 2012. He is currently an Associate Professor with the School of Mechanical Engineering, North China Electric Power University. His research interests include fault diagnosis, signal processing, and testing technology.

XIAOLONG WANG was born in Heilongjiang, China, in 1989. He received the Ph.D. degree from North China Electric Power University, China, in 2016. He is currently a Lecturer with the School of Mechanical Engineering, North China Electric Power University. His research interests include signal processing, pattern recognition, and fault diagnosis.

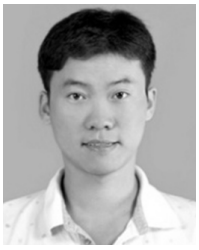

LONGJIANG DOU (Member, IEEE) was born in Hebei, China, in 1988. He received the Ph.D. degree from North China Electric Power University, China, in 2019. He is currently a Lecturer with the School of Mechanical Engineering, North China Electric Power University. His research interests include fault diagnosis of circuit breaker and dynamics of mechanical systems.